Journal Pre-proofs

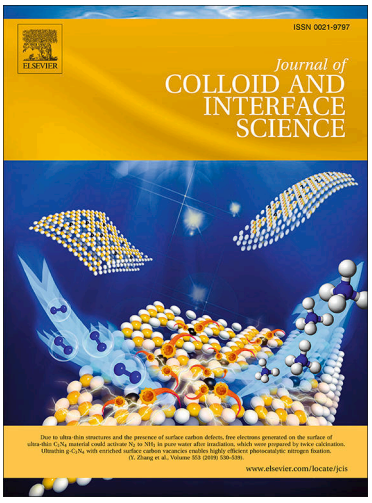

New insights into the interactions between asphaltene and a low surface energy anionic surfactant under low and high brine salinity

Sajad Kiani, Daniel R Jones, Shirin Alexander, Andrew R. Barron

PII: S0021-9797(20)30299-X
DOI: https://doi.org/10.1016/j.jcis.2020.03.018
Reference: YJCIS 26133

To appear in: *Journal of Colloid and Interface Science*

Received Date: 26 August 2019
Revised Date: 2 March 2020
Accepted Date: 5 March 2020

Please cite this article as: S. Kiani, D.R. Jones, S. Alexander, A.R. Barron, New insights into the interactions between asphaltene and a low surface energy anionic surfactant under low and high brine salinity, *Journal of Colloid and Interface Science* (2020), doi: https://doi.org/10.1016/j.jcis.2020.03.018

Submitted to J. Colloid Interface Sci.

New insights into the interactions between asphaltene and a low surface energy anionic surfactant under low and high brine salinity

Sajad Kiani,[a] Daniel R Jones,[a] Shirin Alexander,*[a] and Andrew R. Barron*[a,b,c]

[a]*Energy Safety Research Institute (ESRI), Swansea University, Bay Campus, Swansea SA1 8EN, UK.*

[b]*Department of Chemistry, Rice University, Houston, Texas 77005, USA.*

[c]*Environmental Engineering, Faculty of Engineering, Universiti Teknologi Brunei, Brunei Darussalam.*

HIGHLIGHTS

- Hyperbranched low surface energy surfactants (LSES) show ca. 2× increase in the original-oil-in-place recovery, as compared to brine flooding.
- In comparison to brine, the addition of LSES dramatically alters the asphaltene aggregate size.
- Unlike the results for brine, the oil recovery profile for LSES-brine flood is not affected by alterations in the brine chemical composition.
- LSES-brine leads to significant changes in contact angles (up to 50°) of the asphaltene coated substrate.

* Corresponding authors at. Energy Safety Research Institute (ESRI), Swansea University, Bay Campus, Swansea SA1 8EN, UK

* E-mail: s.alexander@swansea.ac.uk (Shirin Alexander); a.r.barron@swansea.ac.uk (Andrew R. Barron).

* ORCHID ID: Sajad Kiani: 0000-0003-1609-6855; Daniel Jones: 0000-0002-4889-9153; Shirin Alexander: 0000-0002-4404-0026: Andrew R. Barron: 0000-0002-2018-8288

ABSTRACT

Hypothesis: The hyperbranched chains on the tail of low surface energy surfactants (LSES) causes lowering of surface free energy and rock wettability alteration, offering significant improvement in oil recovery in asphaltene oil reservoirs.

Experiments: Oil sweep efficiency was determined by fluid displacement in pure brine and LSES-brine solutions in a microfluidic pattern that was representative of a sandstone cross-section. Interfacial tension (IFT), wettability alteration, and Raman and X-ray photoelectron spectroscopy (XPS) were used to measure the changes of asphaltene interactions with oil-aged substrate after surface treating with brine and surfactant-brine solutions.

Findings: The hyperbranched LSES yielded a significant increase in the original-oil-in-place (OOIP) recovery (58%) relative to brine flooding (25%), even in the presence of asphaltene. Raman spectra showed the LSES-brine solutions to be capable of causing change to the asphaltene aggregate size after centrifugation treatment.

Keywords: hyperbranched surfactants, wettability alteration, asphaltene, enhanced oil recovery

1. Introduction

Asphaltene characterized by some as the 'cholesterol' of crude oil, is the supramolecular hydrocarbon component of crude oil comprising polycyclic aromatic hydrocarbon (PAH) and acidic compounds, exhibiting high surface activity. Asphaltene can be deposited on the reservoir rock, wellbore, and the surface facilities in the form of islands [1, 2] or archipelagos of multiple PAH molecules [3], causing a significant decrease in the reservoir fluid pressure and an incompatible mixture of fluids [4]. In order to decrease asphaltene aggregation, suitable chemicals are added to increase its solubility, the most common of which used by producers are commercial inhibitor solvents such as toluene, xylene, naphtha, and kerosene [5-7]; however, despite the efficiency of these readily available chemicals, they have significant drawbacks such as costly

pipeline blockages, causing a decrease in oil production flow-rate, water/oil emulsion stabilization, an increase in the fluid channeling, and problems in the refining process [8, 9]. In order to resolve these issues, commercial and novel chemicals may be integrated by changing and decreasing the conformations of benzene dimers in the asphaltene compound [10]. Recent experiments have shown that by changing the thermodynamic equilibrium of asphaltene on the substrate, an increase in oil sweep efficiency of 10–20% can be obtained [11, 12].

Novel technologies including polymer, surfactant, and nanoparticle treatments are currently being developed for both thermal and non-thermal enhanced oil recovery (EOR) scenarios [13-19]. Irrespective of the choice of additive, they are designed to change the interactions within the solid-liquid interface in order to increase mobility ratio (M) and capillary pressure (P_c), thereby lowering asphaltene accretion. For the surfactant process specifically, low to high carbon chains such as zwitterionic, anionic, cationic, and non-ionic are shown to be extremely efficient in high asphaltene content [19-22]. Of particular interest is the ability of these technologies to create a new nanoscale surface layer whilst decreasing interfacial tension (IFT) values by 4-6 order of magnitude [23]. Low-molecular-weight alkylbenzene-derived amphiphiles at the interfaces can enhance asphaltene stabilization via the use of either the polar head group or the length of the alkyl tail [24]. The polar moiety of surfactant attaches to the asphaltenes molecules, and the alkyl tails of surfactant molecules offer steric repulsion that impedes further molecule sheet stacking and stabilizes the fused aromatic ring system [24].

Static adsorption analysis has shown that through the addition of amphiphilic headgroups, a significant increase in the acid-base attraction between asphaltene and amphiphiles may be achieved [24]. These results also suggest that increasing the surfactant's tail length yields a corresponding decrease in the acid-base attraction around asphaltene molecules. Therefore, there exists an optimum amphiphilic tail length for which the number of stable steric layers around asphaltene molecules is maximized (i.e., a minimum of six carbon for p-alkylphenol's tail) [24]. Despite extensive studies, the role of stabilized branched anionic surfactant on simulated rock substrates has yet to be reported under conditions of either low or high salinity. The existence of branched chains on the tail of surfactants causes: (a) lowering surface energy tension; (b) rock wettability alteration; and (c) improvement in the fluid viscoelasticity behavior [25]. There are very few published papers exploring the effects of surfactant in asphaltene oil reservoirs (see Table S1, Supplementary Material) [19, 22].

Submitted to J. Colloid Interface Sci.

The present authors have recently reported the synthesis of a cost-effective and environmentally friendly branched anionic low surface energy surfactant (LSES) surfactant [**I**, $iC_{18}S$(FO-180)], and demonstrated its use for increased fluid transport in both low and high brine solutions, this is a significant result for only a single chain surfactant compared to other type of surfactants [27, 28]. The branched surfactant, $iC_{18}S$(FO-180), was chosen because of its effective chain length, ability to reduce the surface tension, and high stability in electrolyte solutions. To understand the interactions that take place in the brine and LSES-brine systems, interfacial tension (IFT) and contact angle measurements were employed. Raman and XPS were used to assess the interactions of the asphaltene molecules with surfactants after surface treating with surfactant-brine and brine solutions; these techniques were utilized to mitigate oil-containing asphaltene surfaces at low to highly ion solutions. The oil sweep efficiencies have been determined by measuring fluid displacements in various LSES-brine and brine solutions in a microfluidic pattern that is representative of a sandstone cross-section.

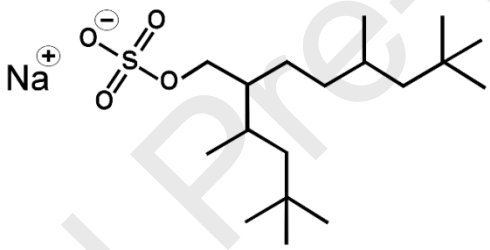

(**I**)

2. Experimental

2.1. Materials

Isostearyl alcohol (Nissan Chemical Industries, Japan) was used to synthesize the $iC_{18}S$(FO-180, critical micelle concentration (CMC) = 2.7 mM, M_W = 362 g.mol^{-1}) using a synthetic method reported previously [28]. Potassium chloride (KCl, > 99% purity), sodium chloride (NaCl, > 99.5% purity), magnesium chloride hexahydrate ($MgCl_2.6H_2O$, > 99% purity), and calcium chloride ($CaCl_2.2H_2O$, > 99% purity) (all purchased from Sigma-Aldrich) were used as received. Distilled deionized water (resistivity = 18.2 MΩ cm, Millipore) was used for preparing synthetic sea water solutions. N-decane, toluene, n-heptane, dichloromethane (DCM), ethanol, and chlorosulfonic acid (all >99%, Fisher Scientific) were also used as supplied. Asphaltene aggregations were conducted using bitumen (Calgary, Canada) to study accumulation of

asphaltene on a glass substrate (extracted by a widely used method (IP143, ASTM D6560), see Table S2-S3 in supporting material for Asphaltene specification).

2.2. *Characterization methods*

Fourier transform infrared attenuated total reflection (FTIR-ATR) analysis of asphaltene aggregates (Figure S1) was made using FTIR Nicolet Nexus 670 ATR in the 600-1800 cm^{-1} region, with 32 scans. Chemical analysis of coated asphaltene substrate was carried out by X-ray photoelectron spectroscopy (XPS) with an Al-K_α X-ray source (1486.6 eV) on a PHI55000 XPS. The survey spectra was measured in the range of 0-1400 eV with 1 eV step size, and 160 eV pass energy. Each core spectrum is deconvoluted into separate Gaussian-Lorentzian components according to the different chemical environments; these components are displayed as solid colored lines, while the Shirley-type background function and the sum of the fitting components are each plotted as a solid black line and the measured data is represented by a thinner black line.

Raman spectra measurements were used to study the average aromatic sheet size by measuring the actual peak position and peak intensities. Spectra's were carried out on the inVia^{TM} confocal Raman microscope, Renishaw. The Raman spectra for all asphaltene coated surfaces were recorded in a range from 500-2000 cm^{-1} at 25 °C (50× long work distance objective). The instrument was equipped with a CDD detector (1064 nm solid state laser, Argon ion laser, 90° scattering geometry, 4 cm^{-1} spectral resolution). Before the Raman measurements, the best care advice is calibration of the laser beam using a clean silicon wafer (reference signal) and removing any fingerprint or dust contamination on the glass slides. Each coated glass carefully was transferred to Raman's slide holder and detected by an ion laser to measure the surface bonding properties (Figure S5). The average of three consecutive runs in six different locations were performed to examine the surface homogeneity and to measure the positions/intensities of the peaks. Molecular structural size of asphaltene was calculated using Tuinstra and Koenig equation (Eq.1) [29]. This model describes the link between the structural size of graphitic carbon material ~~with~~ and both G and D1 bands. The asphaltene aromatic sheet was then calculated when the G band is within the wavenumber range of 1575-1610 cm^{-1}, Eq. 1, whereas asphaltene structural parameter (L_a) were calculated with the integrated intensities of G and D band (I_G and I_{D1}).

$$\text{Diameter, } L_a\,(\text{nm}) = 4.4\frac{I_G}{I_{D1}} \qquad (1)$$

Submitted to J. Colloid Interface Sci.

2.3. *Surface and Solution preparation*

The working surface was made of glass to simulate sandstone rock. The glass was crushed and then sieved (sieve No. 70, 0.210 mm) and the larger particles discarded. The asphaltene onset (beginning point of asphaltene separation from oil) was determined by mixing heptane/toluene solutions (70:30 v/v%) to oil containing asphaltene aggregates. This facilitates homogenous asphaltene accretion on the surface. The remaining glass was then immersed in the oil phase (n-decane + 200 mg asphaltene in heptane/toluene) and left refluxed under 110 °C for 45 days. Afterwards, the glass particles (0.1 g) were transferred into the vials, which each contained 10 mL of the solution. They were then vigorously shaken for 5 min and then centrifuged at 3000 rpm for 30 min to reach an equilibrium condition. The XPS and Raman measurements were taken after the above-mentioned process to confirm the position/intensities of the asphaltene peaks. The brine and surfactant-brine solution preparation and compositions are given in details in the Supplementary Material and Table S5).

2.5. *Adsorption analysis*

Static adsorption isotherms were carried out according to Ahmadi et al experiments [16]. Initially, ordinary glass substrate crushed, and 80 mesh size applied to a filter to obtain the smallest crushed glasses. The crushed glasses were refluxed and aged in oil (n-decane/asphaltene) at 110 °C for 10 days. Then, for each adsorption analysis, 0.5 g of modified crushed glasses were added to 15 ml solution and centrifuge for 30 min at 3000 rpm. Supernatant liquid portion were collected to measure residual surfactant concentration for each [16]. The adsorption isotherms (Q) have been calculated based upon the general adsorption equation (Eq. 2), where Q is the amount of surfactant adsorption ($mg.g^{-1}$) on the solid substrate, m_{Total} and m_{Glass} indicate the total mass of solution (g) and crushed glass (g) respectively, C^0 and C represent the initial and final surfactant concentration ($mg.L^{-1}$) before and after equilibrating adsorption on the crushed glass, respectively. C^0 and C concentration measurements were carried out using electrical conductometer measurements to record the exact amount of surfactant concentrations in different system.

$$Q = \frac{m_{Total.}\,(C^o - C)}{m_{Glass}} * 10^{-3} \qquad (2)$$

Furthermore, Freundlich model (Figure S4 and eq. S1 in supporting material) as a non-linear adsorption equation was used to assess maximum surfactant adsorption on the surface. This equation states that multilayer adsorption (q_e) will exponentially occur on the solid surface.

2.6. *Surface/interfacial tension, and contact angle measurements*

Measurements for air-fluid (surface tension) and fluid-fluid (interfacial tension) were made using DSA25 Expert Drop Shape Analyzer, with ADVANCE software (KRÜSS GmbH) equipped with the automated camera at 25 °C. Both surface tension and IFT measurements were repeated five times to minimize errors. In surface tension measurements, the syringe of a hypodermic needle was filled with 1 mL of the aqueous solution, calibrated, then placed in the chamber for 5 min (be equilibrated), and loaded gently. The pendant drop method was applied to measure surface tension values. The droplet profile shapes, each time were fitted by the Young−Laplace equation using a contour-fitting algorithm. Also, IFT measurement (see Fig S7 and S8) was performed while the needle was filled with 1 mL solution, equilibrated, and immersed in the oil phase (n-Decan + 200 mg asphaltene). Dynamic IFT and contact angle of the solutions (Table S6) were carried out on the substrate and assessed using a pendant drop and sessile drop method over 1000 sec. at ambient temperature and 35% humidity. The Contact angle measurements for all experiments were performed after asphaltene ageing on the substrates.

2.6. *Microfluidic analysis*

Visual microfluidic experiments were used to assess fluid displacement and the physical phenomenon taking place when brine and surfactant/brine comes in contact with the oil containing asphaltene aggregates. The oil sweep efficiencies were discussed after each flooding. The simulated sandstone rock etch pattern was made using a CO_2 laser as reported by Kiani et al. [27]. Darcy's law equation was used to calculate the effectiveness of the porosity and permeability (φ = 15%, κ = 7.5 mD, w = 10 cm, h = 0.2 cm). The schematic of the 2D microfluidic pattern in this experiment is shown in Fig. 1. An ultralow flow rate Quizix pump was used to inject fluids (0.0005 $cm^3.min^{-1}$) and a pressure transducer was used to measure subtle variations in pressure. Besides, a high-quality camera was situated above the pattern to capture the fluid movements. For each microfluidic test, different solutions with varying injection volumes were injected using the Quizix pump through the system. Firstly, the micro-model is saturated with brine to allow the system to reach the initial water saturation (S_{wi} = 100%). The micromodel was saturated by water and is free

of air and bubble. Then, oil containing asphaltene aggregates were injected through the pore channels to reach the initial oil saturation (S_{oi} = 100%). Oil-wet state of micromodel was achieved by oil (asphaltene) ageing for one week. In the last step, pre-prepared brine and LSES/brine solutions were flooded at the constant flow rate of (0.0005 $cm^3.min^{-1}$) into the pattern. To assess oil recovery factors, residual oil saturations were analysed by observing the difference between initial (before each measurement) and remaining oil after each flooding using the "3D object counter" function of ImageJ software. The micropattern was cleaned and dried by immersion in a mixture of distilled water and acetone at 70 °C.

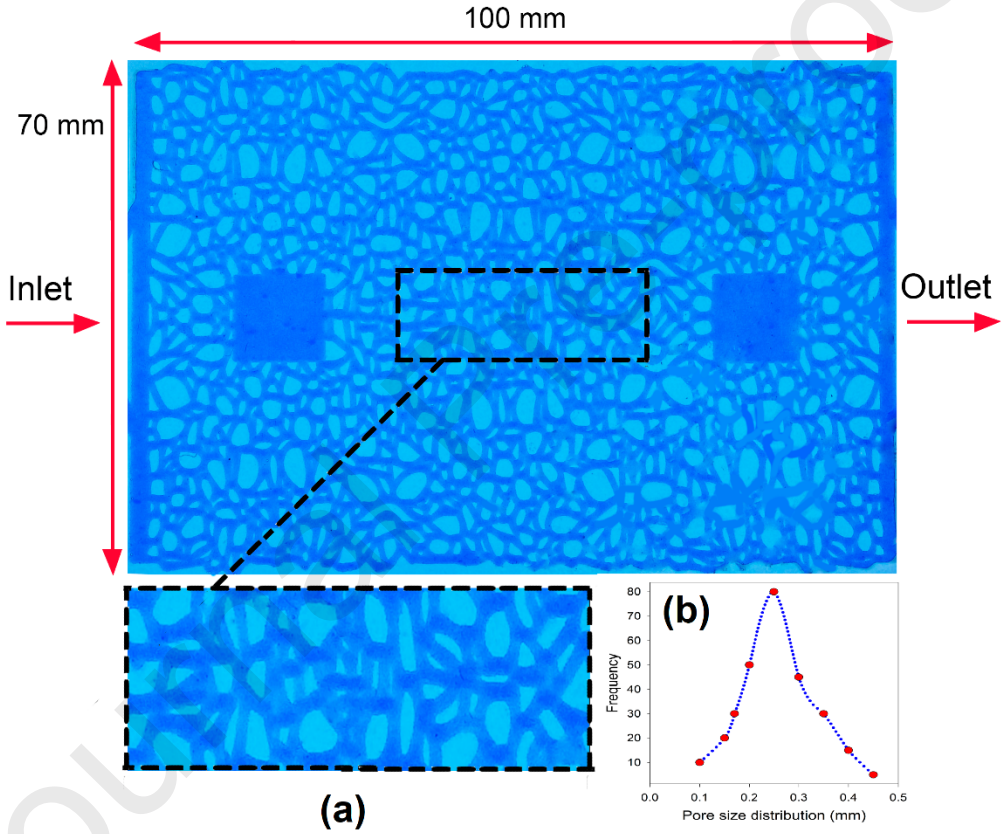

Fig. 1. 2D image of the sandstone microfluidic channel saturated with water (S_{wi}=100%) calculated using the areal sweep efficiency through the microchannel network (from the left to right). The magnified 2D image of the pores (a) and pore throat size distribution (b) of the etched micromodel are also shown.

3. Results and discussions

3.1. Effects of brine and LSES-brine solution on IFT and surface wettability of asphaltene-oil solution

The main parameters of the synthesized highly branched surfactant (branching factor of 7), $iC_{18}S$(FO-180), are summarized in supporting information Table S4. In pure water LSES has a limiting surface tension (γ_{cmc}) of 25.5 $mN.m^{-1}$ (coinciding with the previously reported value of γ_{cmc} = 24.5 $mN.m^{-1}$) and CMC of 2.7 mM [28].

To assess the adsorption of $iC_{18}S$(FO-180) on asphaltene coated surfaces, static adsorption measurements were conducted in three surfactant concentrations (above, at, and below CMC). Static adsorption analysis displays the minimum adsorption of surfactant at and below the CMC value, whereas above CMC shows the highest amount of adsorption (Figure S4). Based on these results and previous results on oil recovery using LSES at CMC [27], we carried out all the measurements in this work at CMC values.

The IFT mechanism of LSES-brine and brine droplet in the oil phase (without the presence of asphaltene) was discussed previously [30] and it was shown that using the LSES in oil−brine system leads to a significant decrease in IFT and volume droplet size. However, the IFT data in the presence of asphaltene are unusual. In this system, synergistic effect on intermolecular interactions in the asphaltene-oil/brine solutions and asphaltene surface-activity behavior result in reduction of IFT values as is shown in Fig S7. Upon addition of the LSES, The IFT values reduced even further from around 10 $mN.m^{-1}$ to around 6 $mN.m^{-1}$ (over 1200 s) for pure water (no brine) systems. The general outcome of the IFT values for the LSES-brine-asphaltene are as follows: PW > SSW-2.5% > SSW-5% > SSW-10% > SSW-50% > SSW-100%. The dynamic IFT (time-dependent) data upon the addition of the surfactant in the asphaltene oil phase is shown in Fig S8, and more information on the IFT reduction mechanism is given in the supporting information.

Change in surface wettability is an efficient way to improve oil sweeping in the porous media.[27, 31] Images of the brine droplets and dynamic contact angle analysis of brine samples on the asphaltene surfaces are shown in Fig. 2a and b respectively. In SSW series, the values show that further increase in brine concentrations cause a slight reduction in contact angle. The effect of brine on contact angle reduction is as follows: PW < SSW-2.5% < SSW-10% < SSW-5% < SSW-50% < SSW-100%. This trend is opposite to the brine contact angle data obtained without the

presence of asphaltene [27]. This is potentially due to ionic and the effect of acid-base interaction in brine-asphaltene-solid system.

Fig. 3 shows the contact angles of LSES-brine droplet on the asphaltene coated substrate. What stands out in Fig. 3, is the significant effect that LSES has on the wettability alteration of the asphaltene coated substrate over 1000 sec. This is due to a more synergistic effect between LSES-brine solutions with asphaltene compared to brine droplets alone on the asphaltene substrate [32].

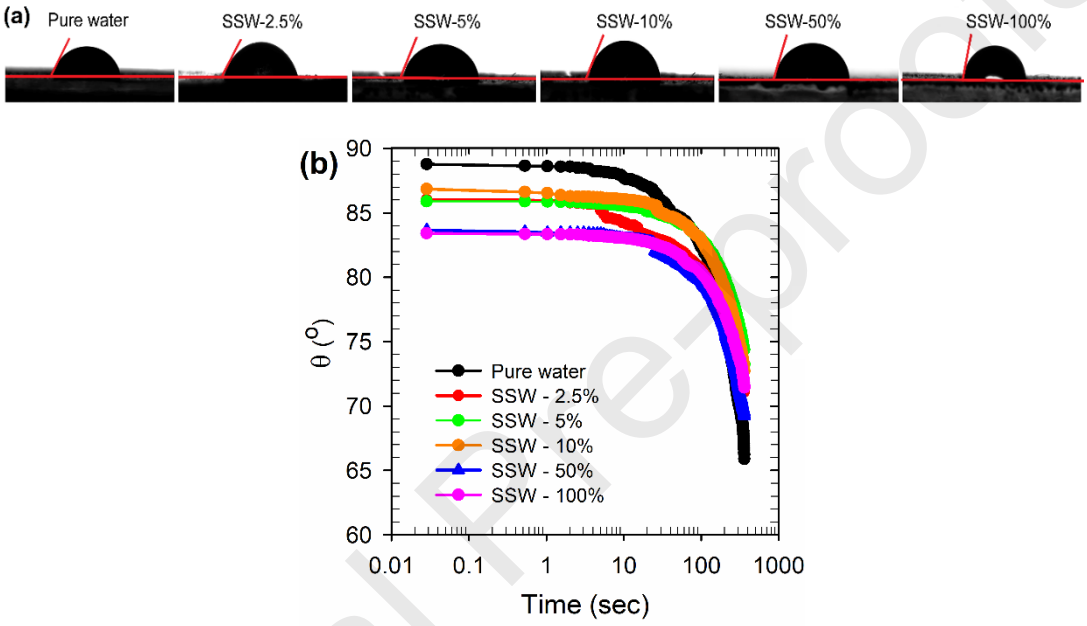

Fig. 2. Images of sessile drops (a) and the dynamic contact angle (b) of brine droplets after a rapid accretion on asphaltene substrate (standard error ±2°).

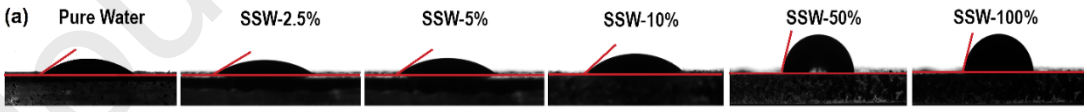

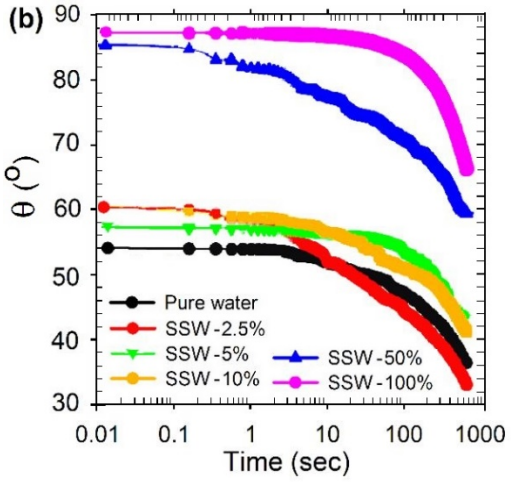

Fig. 3. Images of sessile drops (a) and the dynamic contact angle (b) of LSES-brine droplets after a rapid accretion of asphaltene on the substrate (standard error ±2°).

These results indicate that (at lower salt concentrations) when the droplet hit the asphaltene surface, the LSES made a thin monolayer on the substrate [30]. The highest and lowest θ values were obtained for SSW-100% and SSW-2.5%, respectively (over 1000 s). The data also show that increasing brine concentrations led to an increase in the contact angle of the surfactant solution on the glass substrates from 30 to 70°. This is due to decrease in polarity between the hydrophobic tail and head in the surfactant upon increasing the brine concentration. The results for DCC and MCC solution (shown in Fig. S10) also displays the variation of contact angle (wettability) in DCC (64° - 21°) and MCC (60° - 21°), respectively. This study clearly demonstrates that optimum LSES-brine concentration has a significant influence on the wettability of the coated asphaltene surface.

3.2. Raman measurements

The advantage of using Raman spectroscopy is that it allows us to gain a detailed understanding of molecular bindings in asphaltene-coated substrate. Raman spectra's of asphaltene aggregates were collected and identified using the D and G bands (key features of graphene bands) [33]. The G band illustrates the stretching vibration of the sp^2 carbon atoms within the aromatic hexagonal sheet, moreover expressing sp^2 atoms in the chain of asphaltene [33]. The D band peak reflects the boundary of an ordered-like asphaltene structure. The analysis was based on the comparison between intensity and band position peaks after brine and LSES-brine solutions treatment.

Prior research has reported on the effect of electrolyte on asphaltene aggregates [34]; however, no previous studies have attempted to investigate these changes on coated asphaltene substrate with Raman spectra. Fig. 4 provides the results obtained from the asphaltene-coated substrate after the centrifugation process with twelve brine solutions. Table S7 displays the summary of asphaltene aggregates including shift peak, integrated peak position, full width at half-maximum ($W_{1/2}$: measured as peak width), and the asphaltene structural parameters (L_a) obtained from the Tuinstra and Koenig equation [29]. Peak position was calculated using the peak center at the half-maximum. One of the most exciting aspects of Fig. 4 is the variation of the D and G band peak position (I_D and I_G) which range from 1264 to 1377 cm^{-1} and 1585 to 1599 cm^{-1}, respectively [33]. As demonstrated in Table S7, the calculated L_a values in brine solutions were within the range of 1.073-2.44 nm. Closer inspection of Table S7 shows that adding further brine on the coated asphaltene sheets resulted in the highest value of L_a. The interaction between asphaltene layers is still not fully understood.

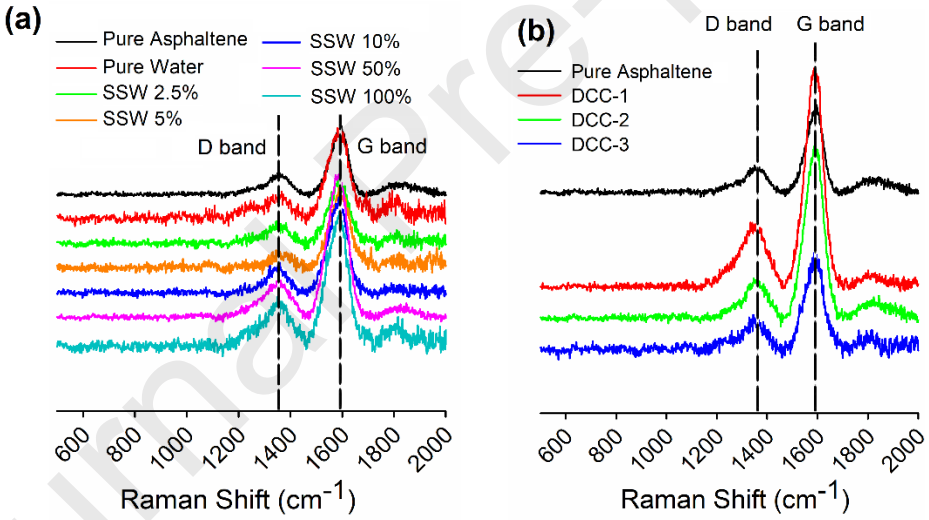

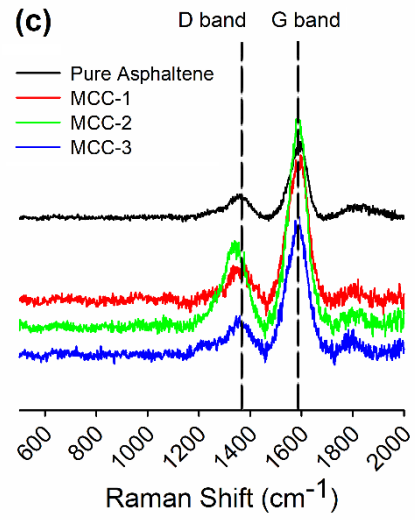

Fig. 4. Raman spectra of the asphaltene surfaces after the adsorption process with brine solutions. The Raman peak intensities show lower asphaltene disordering after centrifugation with brine, although it caused a change in I_D and I_G values within the range of 1264 to 1377 cm^{-1} and 1585 to 1599 cm^{-1}, respectively.

The results displayed on Table S7 show the occupied aromatic molecules are lowest in low brine solutions (pure water to SSW-5%) compared to higher brine solutions. What we know about the D band peak position is based upon the vibrational mode of a disordered graphitic lattice with an A_{1g} symmetry, that investigates how carbon atoms are disordered [36]. While the G band peak position emphasizes the changes in aromatic rings in vibrational mode with E_{2g} symmetry [37]. Raman pick intensities in Table S7 shows the addition of further brine results in a sharp increase in G band peak, this indicates the presence of at least some short-range order of the aromatic sheets, which leads to increased asphaltene fused rings on the substrate (L_a = 1.835 nm) [35]. The current results in Fig. 4 are significant, in at least two major aspects. The first being that optimum brine solution (SSW-2.5%) depicts low asphaltene aromatic sheet size (0.749 nm), the second being greatly increased D and G-band positions as opposed to other brine solutions. These results show that brine significantly affects the aromatic rings of asphaltene on the substrates at low salinity water flooding.

Fig. 5 provides the results obtained from the asphaltene-coated substrate after the centrifugation process with LSES-brine solutions, in order to determine the asphaltene peak shifts and intensities. As can be seen in Fig. 5, there were small changes, yet significant shifts in Raman and band

positions, as well as reduction of asphaltene aggregate size (L_a) after LSES-brine treatment, when compared with the brine solutions. The results of these experiments reveal that the D and G band peak position varies from 1335 to 1398 cm^{-1} and 1576 to 1593 cm^{-1}, respectively [33]. It can be seen from the data in Table S8 that the reason behind these changes lays with the interaction between surfactant and asphaltene surface in the same conditions. These results provide direct evidence that disorder within asphaltene molecules increases on the substrate after LSES-brine solutions.

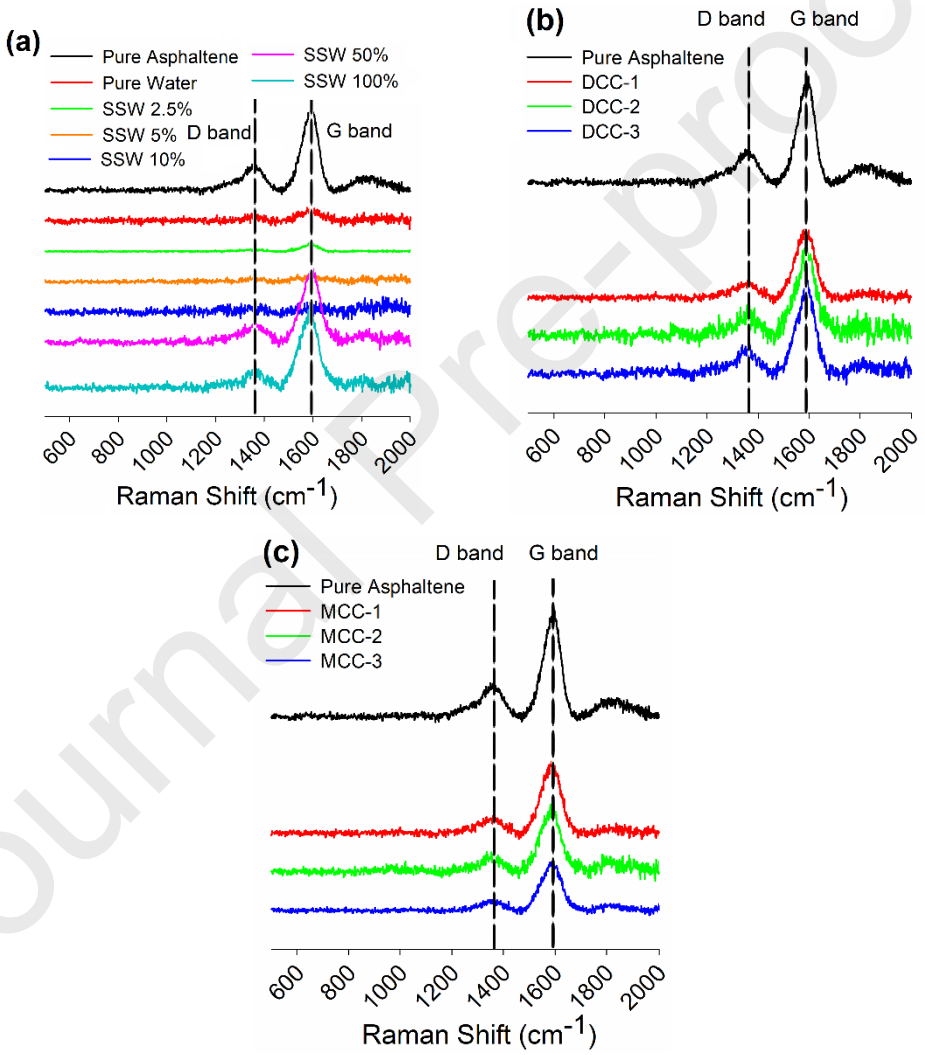

Fig. 5. Raman spectra of the asphaltene surfaces after the adsorption process with LSES-brine solutions. The Raman peak intensities show lower asphaltene disordering after centrifugation with brine, although it caused a change in I_D and I_G values within the range of 1335 to1398 cm^{-1} and 1576 to 1593 cm^{-1}, respectively.

Submitted to J. Colloid Interface Sci.

3.3. XPS measurements

To investigate the effect of the surfactant and brine on the chemical composition of the deposited asphaltene, the XPS spectra of asphaltene was measured according to asphaltene aggregate interactions with 2.5% brine (SSW-2.5%) and LSES-brine solutions (LSES/SSW-2.5%) as a model compound. The survey (Fig. 6 a and b), C 1s, O 1s and Si 2p spectra of the two samples are shown in Fig. 6. The similarity between the two sets of measurements suggests that the presence of LSES only had a slight influence on the composition of the aggregate. The C 1s spectra of both LSES-brine solutions SSW-2.5% and brine SSW-2.5%, depicted in Fig. 6c and d, respectively, are comprised of three components: in addition to the contribution from aliphatic carbon atoms at a binding energy of *ca*. 284.8 eV [38-42], the components at *ca*. 286.6 eV and *ca*. 288.7 eV correspond to C-O and O-C=O chemical environments respectively [38-43]. Within the O 1s spectra in Fig. 6e and f, the primary component at *ca*. 532.2 eV is predominantly attributable in each case to C-O functional groups [44], while the adjacent contribution at ca. 533.9 eV is associated with C=O groups [40]. Finally, Fig. 6g and h show that both samples contained a significant quantity of silicon; in each case, the component at *ca*. 102.1 eV is indicative of C-SiO_x environments, while the smaller contribution at *ca*. 103.4 eV suggests the presence of SiO_2 [38,39,41]. It should be noted that whilst silicon-containing environments are expected to contribute to the C 1s and O 1s spectra, the small quantity of silicon in the samples makes it difficult to discern such contributions amidst the more dominant organic components.

Despite the similarities between the XPS spectra in both samples, there exist some important differences. The relative proportion of silicon, for example, was significantly higher in the LSES/brine solution (SSW-2.5%) sample: silicon-containing species comprised 11.4 at% of this material, compared with 6.3 at% in the case of brine solution (SSW-2.5%). Moreover, while the two materials contained similar quantities of oxygen and aliphatic carbon environments, there was a marked difference in the proportion of C-O and O-C=O groups: whereas these environments respectively accounted for 7.2 at% and 2.7 at% of the LSES-brine SSW-2.5% sample, brine SSW-2.5% contained C-O and O-C=O concentrations of 11.0 at% and 5.6 at%, respectively. This dramatic reduction in C-O and O-C=O % when in the presence of surfactant

can be attribiuted to the ability of the surfactant itself to change asphaltene interaction on the surface.

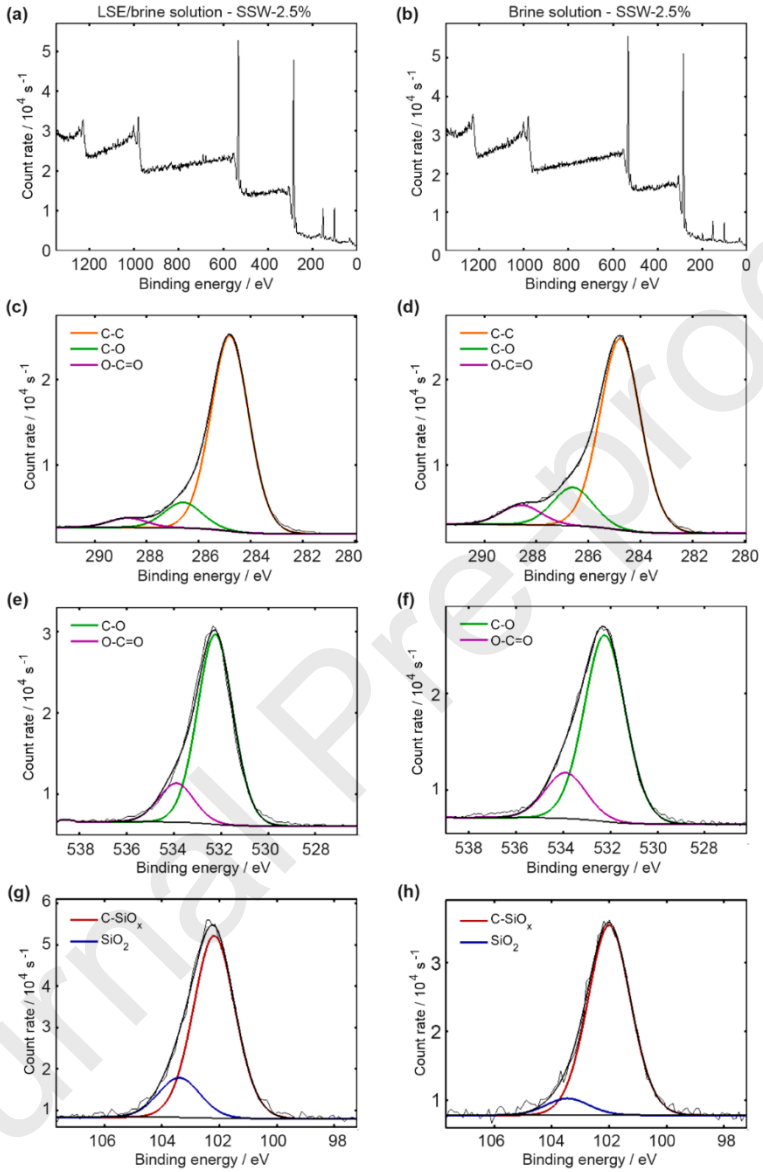

Fig. 6. XPS survey spectra from asphaltene samples deposited from solutions of (a) LSES-brine SSW-2.5% and (b) brine SSW-2.5%. Measurements from LSES-brine SSW-2.5% of the C 1s (c), O 1s (e) and Si 2p (g) core levels are also shown, in addition to the corresponding C 1s (d), O 1s (f) and Si 2p (h) core spectra of brine SSW-2.5%.

3.3. Oil recovery profiles

This study began with two questions: One of which has already been answered by the effect of LSES-brine and brine solution that has a particular effect on disordering and the size of asphaltene aggregates on the substrate. The second, is to decipher how much oil can be pushed out in heterogenous porous media in solutions, as previously mentioned. A series of brine micro floods and LSES-brine solutions were performed to measure the improvement in oil recovery within the porous media.

Fig. 7 displays the results obtained from brine flooding in polar oil components after three pore volume (PV). From Fig. 7 it is apparent that the SSW-5% reported greater oil recovery (23.5%) than other brine flooding. What is interesting about the oil recovery values in Fig. 7a is that the addition of further brine resulted in greater oil sweep efficiency up to SSW-5%, above this, the amount of oil recoveries begins to decline. The oil sweep efficiencies fell to 18%, 12.5%, and 12% in SSW-10%, SSW-50%, and SSW-100% by the end of brine micro flooding. It has been found that in higher brine SSW solutions, ion interactions within fluid-fluid and rock-fluid interfaces created a complicated multiscale system, that caused further asphaltene precipitation on the substrate. The results as shown in Fig. 7 correspond to the Raman spectra results on asphaltene aggregates shown in Table S7: More asphaltene aggregates can be deposited beyond the pores by adding further brine concentrations, leading to decreased oil recovery values. Following this, an increase in their aggregate size is to be expected in this system (Table S7). One reason behind the decline in oil sweep efficiency is the presence of strong ion bonding in the asphaltene-brine-substrate system, which leads to a deterioration in the asphaltene accretion. The cause of ion bonding is most likely a result of the adsorption of multivalent cations on the substrate, although, this has been the subject of intense debate within research groups and oil companies. We know that the main cause of fluid inhibition lies with the formation of the organometallic complexes and an oil-wet state on the rock surface. Chemical-integrated solutions are specifically designed for the breaking and forming of this interaction, on the way toward decreasing the strong interaction on the fluid-solid and further oil liberation on the surface [44-46].

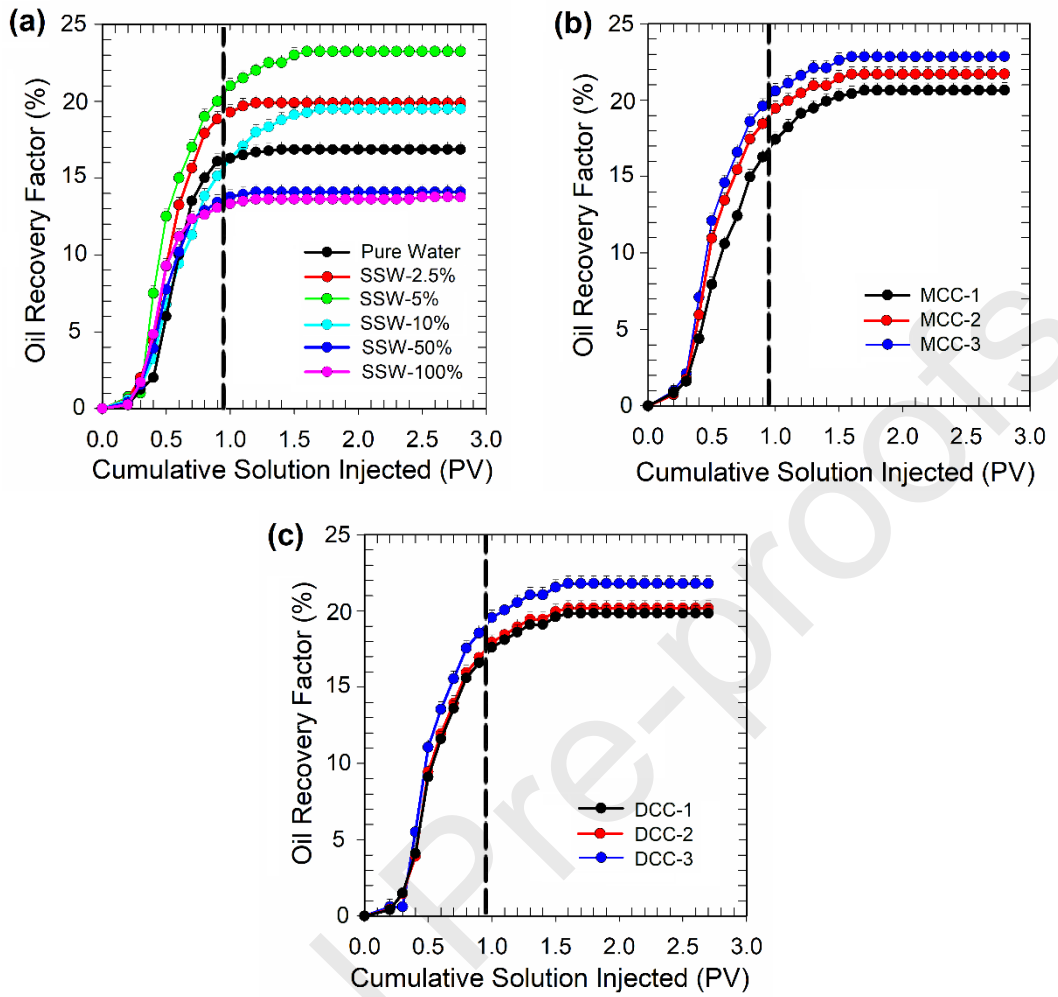

Fig. 7. Oil recovery profiles in pure brine solution (in the presence of asphaltene) using a complex pattern of glass micromodel in (a) SSW series with increased brine concentration from PW to SSW-100%, (b) MCC at various divalent cation concentrations, and (c) DCC at different monovalent cation concentrations.

Fig. 8 provides the results obtained from the micro flooding experiments of LSES-brine flooding analysis. As shown in Fig. 8, greater oil sweep efficiencies were obtained with LSES-brine compared to brine flooding. Maximum oil recovery was obtained by LSES/SSW-5% (~58%). However, as the brine concentration increased, the recovery values decreased to 36 % (after ~1 PV). Strong, attractive ionic interactions in asphaltene-brine-substrate system are achieved following higher brine solutions in SSW-50% and SSW-100%. The oil recovery factor in SSW-50% and SSW-100% were obtained by micro flooding at 41% and 37%, respectively. These results

suggest that the divalent cations in brine solutions led to the promotion of electrostatic forces in the LSES solution, while the monovalent cations caused an increase in repulsive electrostatic forces at the same condition [32]. These findings indicate LSES creates a new layer on the asphaltene substrate, which leads to changes in wettability alteration. What is of great importance here, is the possible displacement of aggregated asphaltene from the oil/water boundary and the solid/water boundary by the LSES surfactant.

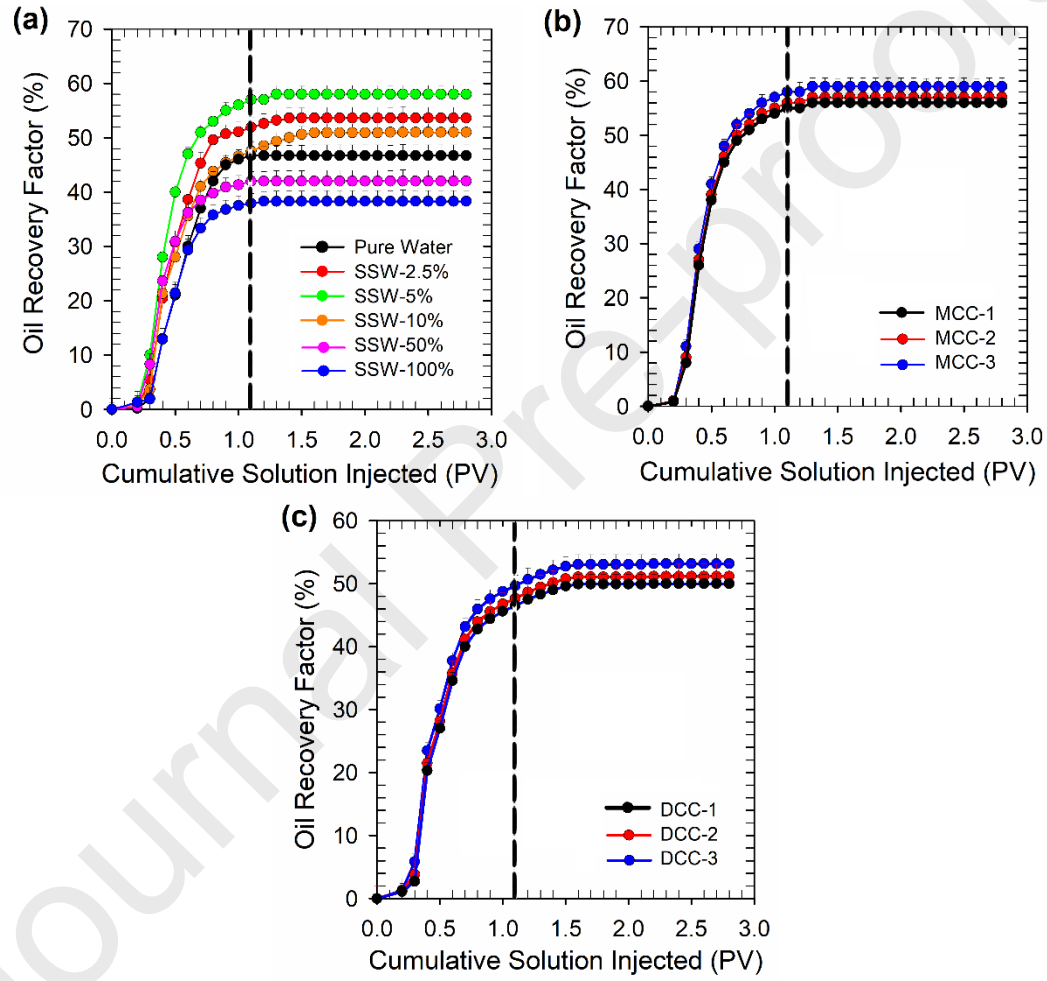

Fig. 8. Oil recovery values in LSES-brine solutions in (a) SSW, (b) MCC, and (c) DCC solution series. Higher bine flooding (SSW-50% and 100%) leads to lower oil recovery values.

A qualitative change of the oil displacement in LSES-SSW-5% (maximum oil recovery) is shown in Fig. 9. During the initial stage of surfactant flooding, homogenous fluid distribution was observed. Further flow channeling along the pattern was detected after 0.5 PV flooding in Fig. 9b.

The main cause of fluid flow channeling is the interaction between oil-brine-surfactant-substrate and low viscosity of the LSES-brine solution [31]. As can be seen in Fig. 9c there is no control of fluid flow in pores and pore-throats after 0.8 PV along the pattern. Applying nanoparticles and polymers in reservoirs containing asphaltene can further minimize the effect of fluid instability and may lead to an increase in the front homogeneity of displacing solutions [31, 46].

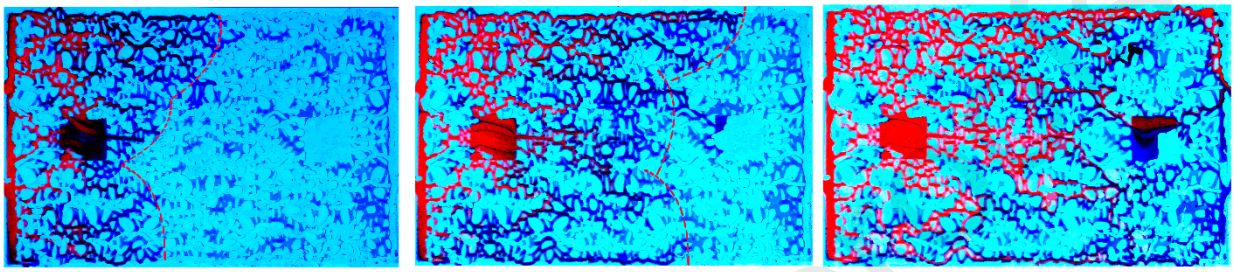

Fig. 9. Top view distribution of solutions in 2D micropattern in optimum LSES-brine solution at three sequential displacement time stages of (a) 0.2 PV (first front), (b) after 0.5 PV and (c) 0.8 PV. The very pale blue, dark blue, and red colors inside the pores represent the oil + asphaltene, water, and LSES-brine solution, respectively.

4. Conclusions

Although in our previous study it was revealed that LSES can be an effective agent for EOR in high salinity and temperature [27], but the consequence of presence of asphaltene was not discussed. As the presence of asphaltene on the reservoir rock can inhibits oil movements and hence effect the oil recovery [1,2], the insight into its interactions with additives such as surfactants becomes vital and essential for EOR formulations. The effect of asphaltene on EOR as well as the value of surfactant in asphaltene oil reservoirs have not been studied extensively. In this study we have examined the presence of hyperbranched low surface energy surfactant, $iC_{18}S$(FO-180), and demonstrated its ability to effectively change asphaltene surface interactions. Based upon Raman spectra data, it appears that LSES-brine solutions can dramatically reduce the asphaltene aggregate size from around 1.4 nm to 0.7 nm for LSES-SSW 5% solutions. This has significant effect on oil recovery. The sweep oil efficiency values exhibited are of only ~25% original oil-in-place (OOIP) recovery after brine flooding; however, the oil displacement increased dramatically to ~58% with LSES-brine solutions. Additionally, the LSES-brine solutions have the ability to lower the

interfacial tension at asphaltene contaminated surfaces and the XPS results confirmed that the reduction in C% in the presence of surfactant can be due to the capability of the surfactant to change asphaltene interaction on the surface. This paper provides a very vital insight for industry as the analysis of the oil recovery show that even in presence of inhibitors such as asphaltene, LSES is capable of increasing the oil recovery significantly and offers a practical alternative to multi-component flooding.

Acknowledgments

Financial support was provided by the Welsh Government Sêr Cymru Programme through Sêr Cymru II Welsh Fellowship part funded by the European Regional Development Fund (ERDF), the Sêr Cymru Chair for Low Carbon Energy and Environment, the Sêr Cymru National Research Network in Advanced Engineering and Materials (NRN-141), King Saud University (under the K(SU)^2 program), and the Flexible Integrated Energy Systems (FLEXIS) operations funded by the Welsh European Funding Office (WEFO) through the Welsh Government. The authors declare no competing financial interest.

Appendix A. Supplementary materials.

Supplementary data associated with this article can be found, in the online version, at DOI: XXXXXX. Composition and characterization of asphaltene with SARA analysis, elemental analysis, FTIR and NMR measurements; asphaltene SEM and AFM image; static adsorption of LSES on the asphaltene coated surface, brine composition, Raman images, contact angle comparison for LSES surfactant on the surfaces, and IFT measurements.

References

[1] H. Groenzin, O.C. Mullins, Asphaltene molecular size and structure, J. Phys. Chem. A 103(50) (1999) 11237-11245.

[2] H. Sabbah, A.L. Morrow, A.E. Pomerantz, R.N. Zare, Evidence for island structures as the dominant architecture of asphaltenes, Energy Fuels 25(4) (2011) 1597-1604.

[3] A. Karimi, K. Qian, W.N. Olmstead, H. Freund, C. Yung, M.R. Gray, Quantitative evidence for bridged structures in asphaltenes by thin film pyrolysis, Energy Fuels 25(8) (2011) 3581-3589.

[4] M. Ghanavati, M.-J. Shojaei, A.R. SA, Effects of asphaltene content and temperature on viscosity of Iranian heavy crude oil: experimental and modeling study, Energy Fuels 27(12) (2013) 7217-7232.

[5] S. Srinivasa, C. Flury, A. Afacan, J. Masliyah, Z. Xu, Study of bitumen liberation from oil sands ores by online visualization, Energy Fuels 26(5) (2012) 2883-2890.

[6] S.K. Harjai, C. Flury, J. Masliyah, J. Drelich, Z. Xu, Robust aqueous–nonaqueous hybrid process for bitumen extraction from mineable Athabasca oil sands, Energy Fuels 26(5) (2012) 2920-2927.

[7] L. He, F. Lin, X. Li, Z. Xu, H. Sui, Enhancing bitumen liberation by controlling the interfacial tension and viscosity ratio through solvent addition, Energy Fuels 28(12) (2014) 7403-7410.

[8] K. Akbarzadeh, A. Hammami, A. Kharrat, D. Zhang, S. Allenson, J. Creek, S. Kabir, A. Jamaluddin, A.G. Marshall, R.P. Rodgers, Asphaltenes—problematic but rich in potential, Oilfield Review 19(2) (2007) 22-43.

[9] M.J. Shojaei, K. Osei-Bonsu, P. Grassia, N. Shokri, Foam flow investigation in 3D-printed porous media: fingering and gravitational effects, Ind. Eng. Chem. Res. 57(21) (2018) 7275-7281.

[10] T.F. Headen, C.A. Howard, N.T. Skipper, M.A. Wilkinson, D.T. Bowron, A.K. Soper, structure of π−π interactions in aromatic liquids, J. Am. Chem. Soc. 132(16) (2010) 5735-5742.

[11] S.S. Betancourt, G.T. Ventura, A.E. Pomerantz, O. Viloria, F.X. Dubost, J. Zuo, G. Monson, D. Bustamante, J.M. Purcell, R.K. Nelson, Nanoaggregates of asphaltenes in a reservoir crude oil and reservoir connectivity, Energy Fuels 23(3) (2008) 1178-1188.

[12] S.M. Hashmi, A. Firoozabadi, Effective removal of asphaltene deposition in metal-capillary tubes, SPE Journal 21(05) (2016) 1,747-1,754.

[13] S. Kiani, M. Mansouri Zadeh, S. Khodabakhshi, A. Rashidi, J. Moghadasi, Newly prepared Nano gamma alumina and its application in enhanced oil recovery: an approach to low-salinity waterflooding, Energy Fuels 30(5) (2016) 3791-3797.

[14] S. Kiani, A. Samimi, A. Rashidi, Novel one-pot dry method for large-scale production of nano γ-Al_2O_3 from gibbsite under dry conditions, Monatsh. Chem. 147(7) (2016) 1153-1159.

[15] F. Moeini, A. Hemmati-Sarapardeh, M.-H. Ghazanfari, M. Masihi, S. Ayatollahi, Toward mechanistic understanding of heavy crude oil/brine interfacial tension: The roles of salinity, temperature and pressure, Fluid Phase Equilib. 375 (2014) 191-200.

[16] M.A. Ahmadi, S.R. Shadizadeh, Adsorption of novel nonionic surfactant and particles mixture in carbonates: enhanced oil recovery implication, Energy Fuels 26(8) (2012) 4655-4663.
[17] G. Cheraghian, L. Hendraningrat, A review on applications of nanotechnology in the enhanced oil recovery part B: effects of nanoparticles on flooding, Int. Nano Lett. 6(1) (2016) 1-10.
[18] N. Pal, N. Saxena, A. Mandal, Studies on the physicochemical properties of synthesized tailor-made gemini surfactants for application in enhanced oil recovery, J Mol. Liq. 258 (2018) 211-224.
[19] P. Zhao, A. Jackson, C. Britton, D.H. Kim, L.N. Britton, D. Levitt, G.A. Pope, Development of high-performance surfactants for difficult oils, SPE Symposium on Improved Oil Recovery, Society of Petroleum Engineers, 2008.
[20] M.M. Shadman, M. Dehghanizadeh, A.H. Saeedi Dehaghani, M. Vafaie Sefti, N. Mokhtarian, An investigation of the effect of aromatic, anionic and nonionic inhibitors on the onset of asphaltene precipitation, JOGPT, 1 (2014) 17-28.
[21] M.J. Shojaei, K. Osei-Bonsu, S. Richman, P. Grassia, N. Shokri, Foam stability influenced by displaced fluids and by pore size of porous media, Ind. Eng. Chem. Res. 58(2) (2018) 1068-1074.
[22] N. Pal, S. Kumar, A. Bera, A. Mandal, Phase behaviour and characterization of microemulsion stabilized by a novel synthesized surfactant: Implications for enhanced oil recovery, Fuel 235 (2019) 995-1009.
[23] P. Raffa, A.A. Broekhuis, F. Picchioni, Polymeric surfactants for enhanced oil recovery: A review, J. Petrol. Sci. Eng. 145 (2016) 723-733.
[24] C.-L. Chang, H.S. Fogler, Stabilization of asphaltenes in aliphatic solvents using alkylbenzene-derived amphiphiles. 1. Effect of the chemical structure of amphiphiles on asphaltene stabilization, Langmuir 10(6) (1994) 1749-1757.
[25] M. Sagisaka, T. Narumi, M. Niwase, S. Narita, A. Ohata, C. James, A. Yoshizawa, E. Taffin de Givenchy, F.d.r. Guittard, S. Alexander, Hyperbranched hydrocarbon surfactants give fluorocarbon-like low surface energies, Langmuir 30(21) (2014) 6057-6063.
[26] D. Subramanian, K. Wu, A. Firoozabadi, Ionic liquids as viscosity modifiers for heavy and extra-heavy crude oils, Fuel 143 (2015) 519-526.

[27] S. Kiani, S.E. Rogers, M. Sagisaka, S. Alexander, A.R. Barron, A new class of low surface energy anionic surfactant for enhanced oil recovery, Energy Fuels 33(4) (2019) 3162-3175.
[28] S. Alexander, G.N. Smith, C. James, S.E. Rogers, F. Guittard, M. Sagisaka, J. Eastoe, Low-surface energy surfactants with branched hydrocarbon architectures, Langmuir 30(12) (2014) 3413-3421.
[29] F. Tuinstra, J.L. Koenig, Raman spectrum of graphite, J Chem. Phys. 53(3) (1970) 1126-1130.
[30] S. Kumar, A. Mandal, Studies on interfacial behavior and wettability change phenomena by ionic and nonionic surfactants in presence of alkalis and salt for enhanced oil recovery, Appl. Surf. Sci. 372 (2016) 42-51.
[31] G. Cheraghian, S. Kiani, N.N. Nassar, S. Alexander, A.R. Barron, Silica nanoparticle enhancement in the efficiency of surfactant flooding of heavy oil in a glass micromodel, Ind. Eng. Chem. Res. 56(30) (2017) 8528-8534.
[32] M.E.J. Haagh, I. Sîretanu, M. Duits, F. Mugele, Salinity-dependent contact angle alteration in oil/brine/silicate systems: the critical role of divalent cations, Langmuir 33(14) (2017) 3349-3357.
[33] O. Alabi, A. Edilbi, C. Brolly, D. Muirhead, J. Parnell, R. Stacey, S.A. Bowden, Asphaltene detection using surface enhanced Raman scattering (SERS), Chem. Comm. 51(33) (2015) 7152-7155.
[34] D. Subramanian, A. Firoozabadi, Effect of surfactants and water on inhibition of asphaltene precipitation and deposition, Abu Dhabi International Petroleum Exhibition and Conference, Society of Petroleum Engineers, 2015.
[35] W.A. Abdallah, Y. Yang, Raman spectrum of asphaltene, Energy Fuels 26(11) (2012) 6888-6896.
[36] O. Beyssac, B. Goffé, C. Chopin, J. Rouzaud, Raman spectra of carbonaceous material in metasediments: a new geothermometer, J. Metamor. Geol. 20(9) (2002) 859-871.
[37] G. Katagiri, H. Ishida, A. Ishitani, Raman spectra of graphite edge planes, Carbon 26(4) (1988) 565-571.
[38] A. Kouloumpis, K. Spyrou, K. Dimos, V. Georgakilas, P. Rudolf, D. Gournis, A bottom-up approach for the synthesis of highly ordered fullerene-intercalated graphene hybrids, Front. Mater. 2 (2015) 10.

[39] F.C. Dos Santos, S.V. Harb, M.-J. Menu, V. Turq, S.H. Pulcinelli, C.V. Santilli, P. Hammer, On the structure of high performance anticorrosive PMMA–siloxane–silica hybrid coatings, RSC Adv. 5(129) (2015) 106754-106763.

[40] S. Roy, T. Das, Y. Ming, X. Chen, C.Y. Yue, X. Hu, Specific functionalization and polymer grafting on multiwalled carbon nanotubes to fabricate advanced nylon 12 composites, J. Mater. Chem. A 2(11) (2014) 3961-3970.

[41] M.-C. Hsiao, C.-C.M. Ma, J.-C. Chiang, K.-K. Ho, T.-Y. Chou, X. Xie, C.-H. Tsai, L.-H. Chang, C.-K. Hsieh, Thermally conductive and electrically insulating epoxy nanocomposites with thermally reduced graphene oxide–silica hybrid nanosheets, Nanoscale 5(13) (2013) 5863-5871.

[42] T. Okpalugo, P. Papakonstantinou, H. Murphy, J. McLaughlin, N. Brown, High resolution XPS characterization of chemical functionalised MWCNTs and SWCNTs, Carbon 43(1) (2005) 153-161.

[43] N. Hordy, S. Coulombe, J.L. Meunier, Plasma functionalization of carbon nanotubes for the synthesis of stable aqueous nanofluids and poly (vinyl alcohol) nanocomposites, Plasma Process. Polym. 10(2) (2013) 110-118.

[44] M.A. Buccheri, D. D'Angelo, S. Scalese, S.F. Spanò, S. Filice, E. Fazio, G. Compagnini, M. Zimbone, M.V. Brundo, R. Pecoraro, Modification of graphene oxide by laser irradiation: a new route to enhance antibacterial activity, Nanotechnology 27(24) (2016) 245704.

[45] P. Hopkins, K. Walrond, S. Strand, T. Puntervold, T. Austad, A. Wakwaya, Adsorption of acidic crude oil components onto outcrop chalk at different wetting conditions during both dynamic adsorption and aging processes, Energy Fuels 30(9) (2016) 7229-7235.

[46] L. He, F. Lin, X. Li, H. Sui, Z. Xu, Interfacial sciences in unconventional petroleum production: from fundamentals to applications, Chem. Soc. Rev. 44(15) (2015) 5446-5494.

Submitted to J. Colloid Interface Sci.

Graphical abstract:

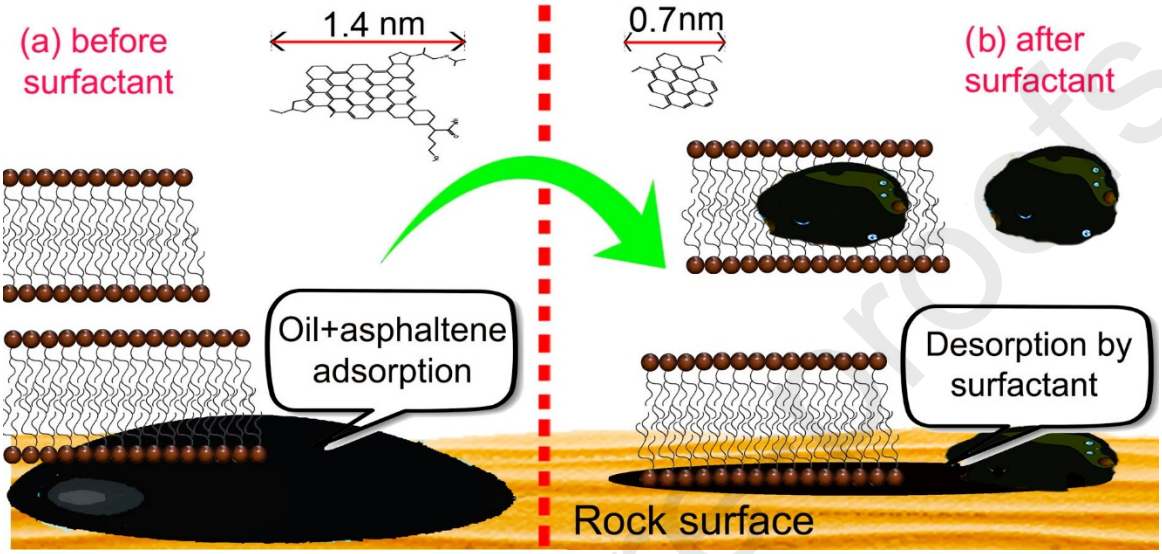

Declaration of interests

☒ The authors declare that they have no known competing financial interests or personal relationships that could have appeared to influence the work reported in this paper.

☐The authors declare the following financial interests/personal relationships, which may be considered as potential competing interests:

Sajad Kiani: Writing - original draft; Conceptualization; Data curation; Formal analysis; Investigation; Methodology

Daniel R Jones: Formal analysis; Investigation; Writing - review & editing

Shirin Alexander: Funding acquisition; Writing - review & editing; Supervision;

Andrew R. Barron: Funding acquisition; Writing - review & editing; Supervision; Project administration; Methodology